Modulation of Enzyme Cascade Activity by Local

Substrate Enrichment and Exclusion on DNA

Nanostructures

Zhicheng Wang †,‡ , Ezry St. Iago-Mcrae † , Alireza Ebrahimimojarad † , Sung Won Oh †,‡ and Jinglin Fu *,†,‡

[†] Center for Computational and Integrative Biology, Rutgers University-Camden, 201 Broadway, Camden, NJ 08103, USA

[‡] Department of Chemistry, Rutgers University-Camden, 315 Penn Street, Camden, NJ 08102, USA

KEYWORDS

DNA nanostructure, multi-enzyme cascade, substrate confinement, aptamers, immobilized enzymes

ABSTRACT

Substrate confinement and channeling play a critical role in multienzyme pathways, and are considered to impact the catalytic efficiency and specificity of biomimetic and artificial nanoreactors. Here we reported a modulation of a multienzyme system with the cascade activity impacted by the surface affinity binding to substrate molecules. A DNA origami modified with aptamers was used to bind and enrich ATP molecules in the local area of immobilized enzymes, thereby enhancing the activity of an enzyme cascade by more than two folds. Alternatively, DNA nanostructure modified with blocked aptamers does not bind with ATP, thereby reducing the activity of the enzyme cascade. The Michaelis-Menten kinetics showed decreased apparent K_M values (~ 3-fold lower) for enzyme nanostructures modified with aptamers, suggesting the higher effective substrate concentration near enzymes due to the local enrichment of substrates. Conversely, increased apparent K_M values (~ 2-fold higher) were observed for enzyme nanostructures modified with blocked aptamers, possibly due to the exclusion of substrates approaching the surface. The similar concept of this modified surface-substrate interaction should be applicable to other multienzyme systems immobilized on nanostructures, which could be useful in the development of bio-mimetic nanoreactors.

1. INTRODUCTION

Cell function relies on a series of cascaded and confined chemical reactions, which are used to carry out important metabolic functions of chemical conversions, energy transformations and signal transductions. Cellular multienzyme cascades are often spatially organized and optimized to facilitate the transport of intermediate substrates for improving efficiency and specificity of reactions. Such examples include scaffold in protein assembly, protein neighbors assembly, metabolons and compartments. The ability to mimic and produce these biological structures in noncellular environment will not only increase our understanding of fundamental life function and evolution, but could also impact a broad range of potential applications to benefit both scientific community and society. In the recent decades, various approaches have been developed to create artificial and biomimetic multienzyme reactors, including cross-linked enzyme aggregates,² co-immobilized enzyme beads,³ synthetic metabolon,^{4,5} polymer vesicles⁶⁻⁸ and virus-like particles. The ability to exert control over biomolecular assembly on the nanoscale is critical to the development of non-living, artificial and biomimetic reactors.

DNA self-assembly has revolutionized the understanding and organization of biomacromolecules on the nanoscale. Began with Ned Seeman's construction of artificial "Holliday" junction, in the past four decades, DNA self-assembly has been widely adopted for the design and fabrication of prescribed and sophisticated 1D, 2D and 3D nanostructures. 11-13 Several breakthroughs in the methodology of DNA self-assembly, such as DNA crossovers, 14 scaffolded DNA origami 15 and DNA bricks 16, have empowered the design capability toward more complex structures and functionality, 17,18 as well as folding nanostructures with single-stranded nucleic acids. 19 Owing to unique features of programmable and prescribed geometry, sequence-addressable assembly and adaption to various bioconjugations, 20 DNA nanostructures hold great

promise to organize complex molecular systems with precise control of spatial arrangements.^{20,21} For example, multienzyme systems were assembled on DNA nanostructures for controlling interenzyme distances,^{22,24} engineering biomimetic swinging arms,^{25,27} and confining enzymes within nanocages.^{28,30} DNA nanostructures can also be used to engineer micro/nano-environment for modulating biochemical activities, such as the stabilized hydration layer³⁰ and decreased local pH.³¹ Using nucleic acids (e.g. aptamers) to bind with enzyme substrates, it enriched substrate molecules on DNA scaffolds, and thereby increasing the activity of attached enzymes.^{32,36} By modifying the surface affinity to small molecule ligands, it is possible to make biomimetic nanoconfinement with the ability to trap substrate molecules for facilitating the substrate channeling in multienzyme systems. DNA-conjugated enzyme complexes were also used to modulate the proximity interaction between enzymes and catalytic partners,³⁷ inhibitors^{38,40} and cofactors^{41,42}, thereby regulating enzyme activities¹ and improving enzyme stabilities.⁴³

Here, we reported to use DNA nanostructures to organize a multienzyme complex with the cascade activity impacted by the surface affinity binding to intermediate substrate molecules. Aptamer modifications were able to bind and enrich ATP molecules near enzymes on a DNA origami, thereby promoting the activity of a kinase cascade. Alternatively, blocker-modified structures were used to exclude ATP molecules from reaching to the origami surface, thereby reducing the cascade activity.

2. MATERIALS AND METHODS

2.1. Materials.

Pyruvate kinase (Type II from rabbit muscle) and hexokinase (from Saccharomyces cerevisiae) were purchased from Sigma, glucose-6-phosphate dehydrogenase (G6pDH) was purchased from

Worthington Biochemical. M13 single-stranded DNA was purchased from Bayou Biolabs. Single-stranded oligonucleotides were purchased from IDT. SPDP (N-Succinimidyl 3-(2-pyridyldithio)-propionate) were purchased from Pierce. ATP-Cy3 was purchased from Jena Bioscience. 10 ×TBS (tris buffered saline) and sodium HEPES were ordered from Sigma.

2.2. Preparation of buffer solutions.

All buffers are prepared in deionized water or distilled.

 $1 \times \text{TAE-}\ 12.5 \text{ mM Mg}^{2+}$ (pH 8.0) contains 40 mM Tris, 20 mM acetic acid, 2 mM EDTA and 12.5 mM magnesium acetate. It is prepared by diluting 100 mL 10 ×TAE into 900 mL deionized water. $10 \times \text{TAE-}125 \text{ mM Mg}^{2+}$ (pH 8.0) contains 400 mM Tris, 200 mM acetic acid, 20 mM EDTA and 125 mM magnesium acetate. 44 1 × TBS- 4 mM Mg $^{2+}$ (pH 7.5) contains 1 × TBS and and 4 mM MgCl₂ with pH adjusted to 7.5.

2.3. Preparation of DNA origami.

Rectangular DNA origami tiles were prepared in $1 \times TAE$ - 12.5 mM Mg^{2+} buffer using published protocols. He priefly, 20 nM single-stranded M13mp18 DNA (7,249 nucleotides) was mixed with a 5-fold molar excess of staple stands and a 10-fold molar excess of anti-anchor strands. The mixture was annealed from 95 °C to 4 °C with the temperature gradient listed in the supporting information Table S1. The excess staple strands were removed by washing the solution in $1\times TAE$ Mg²⁺ buffer (pH 8.0) with 100 kD-cutoff Amicon filters (500 μ L) for three times. The concentration of DNA origami solution was quantified by absorbance at 260 nm, assuming an extinction coefficient of $\sim 109119009 \text{ M}^{-1}\text{cm}^{-1}$. The detailed design of DNA origami structures was shown in the supporting information Figure S1 and Table S4-S7.

2.4. Binding affinity assay by anisotropy and aptamer switch.

ATP-binding aptamer was purified with denatured gel as described in the previous publication. Anisotropy experiment was carried out by the polarization filter of Cytation 3 multimode reader (Biotek/Agilent). $0.5~\mu$ M ATP-Cy3 was added with aptamer ranging from 0- 32 μ M. The fluorescence anisotropy value was calculated with the equation:

Anisotropy value= $(parallel - perpendicular)/(parallel + 2 \times perpendicular)$

For aptamer-complement switch, Cy5 and Iowa Black® RQ labelled strands were used for fluorescence quenching and recovery measurement. 10 nM aptamer-complement duplex was prepared in $1 \times TBS-4$ mM Mg²⁺ buffer. The mixture was annealed from 90 °C to 15 °C with the temperature gradient shown in the supporting information Table S2. The structure was then incubated with ATP from 0- 1300 μ M for 30 minutes prior to the read of fluorescence. The sequences design and details were shown in the supporting information Figure S2 and Table S4-S5. All DNA strands were purified with denatured gel as described previously.⁴⁴

2.5. Enzyme-DNA conjugation.

SPDP was used to crosslink enzymes with DNA strands as described previously. HEK was conjugated to WN1 strand (5-NH₂-TTTTTCCCTCCCTCC-3) and PK was conjugated to WN2 strand (5-NH₂-TTTTTGGCTGGCTGG-3). Enzyme solution was first incubated with SPDP (1:5 molar ratio) in 50 mM HEPES buffer (pH 8.5) for one hour. Excess SPDP was removed by washing the solution with 30 kD-cutoff Amicon filters for three times. Next, SPDP-modified protein was conjugated to thiol-modified DNA (8-fold molar excess) through a disulfide bond exchange of the activated pyridyldithiol group. The reaction mixture was incubated in 50 mM HEPES buffer (pH 7.5) for one hour. Finally, the excess DNA was removed by washing the solution with 30 kD-cutoff Amicon filters. DNA-conjugated enzymes were further purified by

anion-exchange HPLC to collect the fraction of enzymes labelled with two DNA strands as described previously.⁴⁴

2.6. Co-assembly of enzymes on DNA origami tiles.

DNA-conjugated PK and HEK enzymes were mixed with DNA origami tiles in 1 × TAE- 12.5 mM Mg²⁺ buffer (pH 7.5) with a molar ratio of 3:1. The solution mixture was cooled from 37°C to 4°C with the temperature gradient shown in the supporting information Table S3.⁴⁴ Then, aptamers and aptamer-complement complexes were introduced onto the enzyme-assembled origami structures. To prepare aptamer-modified origami, aptamer strands (2:1 molar ratio) and apatmer complement strands (4:1 molar ratio) were added into the solution and incubated for 30 mins at room temperature (RT). The sequences details were shown in the supporting information Figure S1 and Table S5.

2.7. Evaluation of enzyme activity.

PK-HEK cascade reaction produces glucose-6-phosphate (Figure 1A), which is analyzed by G6PDH-catalyzed NADH production. Enzyme assay was performed in 1×TBS, 4 mM Mg²⁺ buffer (pH 7.5) with the addition of a substrate mixture of 500 μ M glucose PEP, NAD⁺, 10 nM G6PDH and a varied ADP concentrations depending on the specific experiments. The optimization of buffer and salt conditions was shown in the supporting information Figure S3. The activity was evaluated by monitoring the increased absorbance at 340 nm resulted from NADH production. Collected reaction curves were fit by GraphPad Prism using Michaelis-Menten equation for apparent K_M ($K_{M,app}$) and V_{max} values.

2.8. Atomic force microscope (AFM) imaging.

DNA nanostructures were imaged in liquid by AFM using the published protocol.⁴⁴ 2 μL of enzyme-origami solution was first deposited onto a freshly cleaved mica surface (Ted Pella,

Redding, CA) and was left to adsorb for 2 minutes. Then, $80 \,\mu\text{L}$ of $1 \times \text{TAE-} 12.5 \,\text{mM} \,\text{Mg}^{2+}$ buffer was added to the Mica for scanning in liquid. $2 \,\mu\text{L}$ of $100 \,\text{mM} \,\text{Ni}^{2+}$ were also added to enhance DNA adsorption on mica. The samples were scanned by the "Scanasyst mode in liquid mode" of Multimode $8 \,\text{AFM}$ (Bruker, Billerica, MA), using "SCANASYST-Fluid + probe".

3. RESULTS AND DISCUSSION

In **Figure 1A**, the general design includes a two-enzyme cascade of pyruvate kinase (PK)⁴⁵ and hexokinase (HEK) 46 that are assembled together on a rectangular M13 DNA origami tile.23 PK catalyzes the production of ATP by transferring a phosphate group from phosphoenolpyruvate (PEP) to a ADP, similarly as its function in glycolysis. Then, HEK uses an ATP to phosphorylated glucose for producing glucose-6-phosphate (G6P). The G6P is detected by a dehydrogenase/NAD assay as described in the method. 41 To enrich ATP molecules near enzymes, multiple ATP-binding aptamers^{47,48} are positioned in the middle path between PK and HEK on the origami surface. In Figure 1B, the assembly of the enzyme complex was characterized by atomic force microscopy (AFM). The co-assembly of PK/HEK pairs on DNA origami tiles (45 nm interenzyme distance) were ~ 80 - 94 % (Supporting Information Figure S4). The right panel showed the similar enzyme-origami structure but modified with 14 aptamers, which formed a bright strip under AFM imaging. Next, we tested the binding of an aptamer to an ATP molecule. In Figure 2A, fluorescence anisotropy measurement characterized that the aptamer bound to a Cy3-labelled ATP in solution with the dissociation constant $(K_d) \sim 6 \mu M$, which was in consistent with the published value for this aptamer.⁴⁸ In Figure 2B, an aptamer-complement duplex was displayed on a DNA origami tile. In this duplex, Cy5-labelled aptamer was quenched by a BHQlabelled complement strand. For 11-nucleotide (nt) complement strand, the aptamer-complement duplex was disrupted by the addition of ATP molecules due to the aptamer-ATP binding, resulting in an increased Cy3 fluorescence. For 15-nt complement strand, the aptamer-complement duplex was too stable to be disrupted by the aptamer-ATP binding, thus, was unable to bind with a ATP. This data demonstrated the regulation of the ATP-aptamer binding on the DNA origami surface. In later experiments, 15-nt aptamer-complement duplex was used as a blocker to prevent ATP from binding to the DNA origami surface. The aptamer also bound to ADP similarly as binding to ATP. Sequence design was shown in the supporting information Figure S2. In Figure 3, a simplified equilibrium model suggested the enrichment of ATP concentrations on the surface of a DNA origami by introducing aptamer modifications. Region close to the aptamers (K_d is assumed at 10 µM) was able to enrich a high local concentration of ATP molecules (within 5 nm), which decayed exponentially to the bulk concentration of 10 µM as the increased distance from the surface. However, the model does not account for avidity effects, dynamic diffusion and electrostatic forces. This steady-state model is used to simply describe the ATP enrichment effect in the local area of aptamer-modified surface. It cannot be used for accurately predicting the exact ATP enrichment and concentration in a reaction-diffusion system.

Next, we experimentally evaluated the effect of aptamer modification for impacting the PK/HEK cascade activity. In **Figure 4A**, the enzyme cascade activity was increased as introducing more ATP-binding aptamers onto the DNA origami surface from 0 to 48. The normalized activity (**Figure 4B**) showed that the nanostructure with 10-aptamer modification boosted the enzyme cascade activity for almost two folds, and nanostructures modified with more aptamers of 24 and 48 enhanced the enzyme cascade activity for more than two folds. To be noted, a structure modified with 14 aptamers showed abnormally lower activity than other aptermer-modified structures. This was attributed to the very closed position between aptamers and enzymes for the 14-aptamer

modification (see the origami design map in the supporting information Figure S1 and Figure S8), thereby, aptamer could inhibit the nearby enzyme by blocking the active site or other local electrostatic and ionic interactions. We also tested the blocked aptamer-complement duplexes for affecting the enzyme cascade activity. As previously discussed in **Figure 2B**, a 15-nt aptamer-complement duplex was unable to bind with a ATP due to the stable hybridization of the duplex. In **Figure 4C**, all structures modified with blocker duplexes showed lower activities than structures modified with aptamers in **Figure 4A**. Normalized activity in **Figure 4D** further showed that enzyme nanostructures modified with 10 blockers or more were even less active than the control enzyme nanostructure without an aptamer modification.

To investigate the mechanism of boosted or inhibited enzyme reactions induced by aptamer modifications, we further evaluated the reaction kinetics for some representative structures. In **Figure 5A**, we compared enzymatic activities of several structures, including non-aptamer modification, 10-apatmer modification, 10-apatmer/blocker modification and 14-aptamer/blocker modification. The result showed that a DNA origami tile modified with multiple ATP-binding aptamers boosted the activity of the enzyme cascade on the nanostructure, while DNA origami tiles modified with blocker duplexes significantly reduced the enzyme cascade activity on nanostructures. In **Figure 5B**, we measured the enzyme activity depending on added ADP concentrations for evaluating the apparent Michaelis constant ($K_{M, app}$) of the overall enzyme cascade reaction. The enzyme nanostructure with 10-aptamer modification showed the smallest apparent K_{M} value of ~ 296 μ M, and the enzyme nanostructure without aptamer modification showed a higher $K_{M, app}$ value of ~ 860 μ M. Enzyme nanostructures modified with aptamer/blocker showed much larger $K_{M, app}$ values of ~ 1060 μ M for 10-aptamer/blocker and ~ 1831 μ M for 14-aptamer/blocker. V_{max} values for all enzyme structures were ranged from 54 μ M to 66 μ M, which

was less variations than apparent K_M values. It suggested that different activities of these enzymes structures were primarily attributed to K_M change, rather than V_{max} variations. The raw reaction curves for fitting were included in the supporting information Figure S5-S7. Free enzymes unassembled on DNA origami showed lower activity than enzymes assembled on DNA origami (supporting information Figure S6), possibly due to the enhancement effect of DNA scaffolds that were reported previously. 20,30,31

If assuming the true K_M and V_{max} of enzymes are not significantly affected by aptamer modifications, the apparent K_M value $(K_{M,app})$ is related to the effective ADP concentration in the local area of enzymes. ADP concentration near DNA origami surface (Ssurf) can be described as: $S_{surf} = S_{bulk} \times \alpha$, where S_{bulk} is the added ADP concentration in bulk solution, α is the surface enrichment factor. For an enzyme reaction on DNA origami, it follows the Michaelis-Menten kinetics as: $V = \frac{V_{max} * S_{surf}}{K_M + S_{surf}}$; where the true K_M and V_{max} are determined by the local concentrations of ADP. However, the apparent K_M value $(K_{M, app})$ is measured by bulk concentrations as: V = $\frac{V_{max}*S_{bulk}}{K_{M,app}+S_{bulk}}$. From these, it can be derived as: $\frac{K_M}{K_{M,app}} = \frac{S_{surf}}{S_{bulk}} = \alpha$. In **Table 1**, the enrichment factor (α) is defined as 1 for the enzyme structure without any aptamer modification. The enzyme nanostructure with 10-apatmer modification showed a decreased apparent K_M than the structure without aptamer modification, thus, α value for this 10-apta structure is \sim 2.9. It indicated a significant enrichment of local substrates on the surface of enzyme-DNA nanostructure. Enzyme nanostructures modified with blocked aptamers showed increased K_M values, with α values of \sim 0.81 for 10-aptamer/blocker and ~ 0.47 for 14-aptamer/blocker, which suggested that substrates were excluded from the surface of enzyme-DNA nanostructures.

4. CONCLUSION

We have designed and demonstrated the assembly of multi-enzyme complexes on DNA nanostructures with the local enrichment or exclusion of substrate molecules. Aptamers were used to modify the surface of DNA nanostructures for enriching or excluding local ATP molecules. This modulation of local ATP concentrations was found to impact the activity of an enzyme cascade reaction, where enhanced enzyme activities were observed for structures modified with ATP-binding aptamers, and decreased enzyme activities were observed for structures modified with blocked aptamers. The aptamer modifications also affected the Michaelis constant of enzymatic reactions. A decreased apparent K_M indicated the enrichment of local substrates by aptamers, and an increased apparent K_M suggested the exclusion of local substrates near enzymes. The similar concept of this modified surface-substrate interaction should be applicable to other multienzyme systems immobilized on nanostructures, e.g. confined enzyme reactions in nanocages, ³⁰ nanotubes²⁴ or microbeads. ³ Advances in aptamer technology, such as SELEX, can also be used to develop new aptamers targeting on various enzyme substrate ligands. Especially, if aptamers can bind more tightly with substrates than products molecules, it could provide more accurate and strong modulation on enzyme activities. The underlying DNA nanostructures provide programmable frameworks for creating complex enzymatic systems with the regulation of activity and specificity, which could find more useful in the development of bio-mimetic reactors for the synthesis of high-value chemicals, the bioenergy conversion and the fabrication of smart materials, as well as regulatory biological circuits for diagnostic and therapeutic applications.

FIGURES

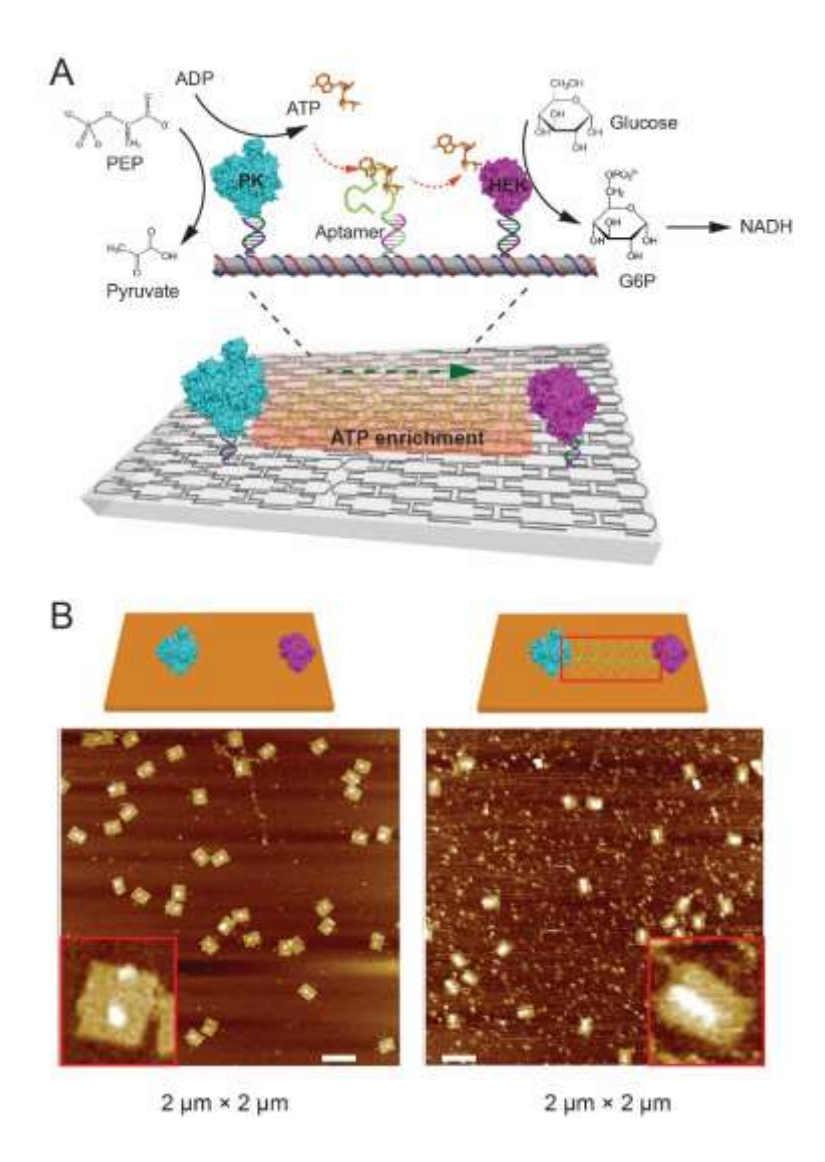


Figure 1. Design and characterization of an aptamer-modified DNA nanostructure providing the enrichment of ATP molecules between two kinases. (A) Schematic of a nanostructured enzyme cascade consisting of PK and HEK organized on a rectangular DNA origami tile. ATP-binding aptamers are modified on the path between the two enzymes. (B) Left: AFM image of the assembled PK–HEK origami tile without the aptamer modification. Right: AFM image of the assembled PK-HEK origami with 14-aptamer modification. Scale bar: 200 nm. Size: 2 μm ×2 μm.

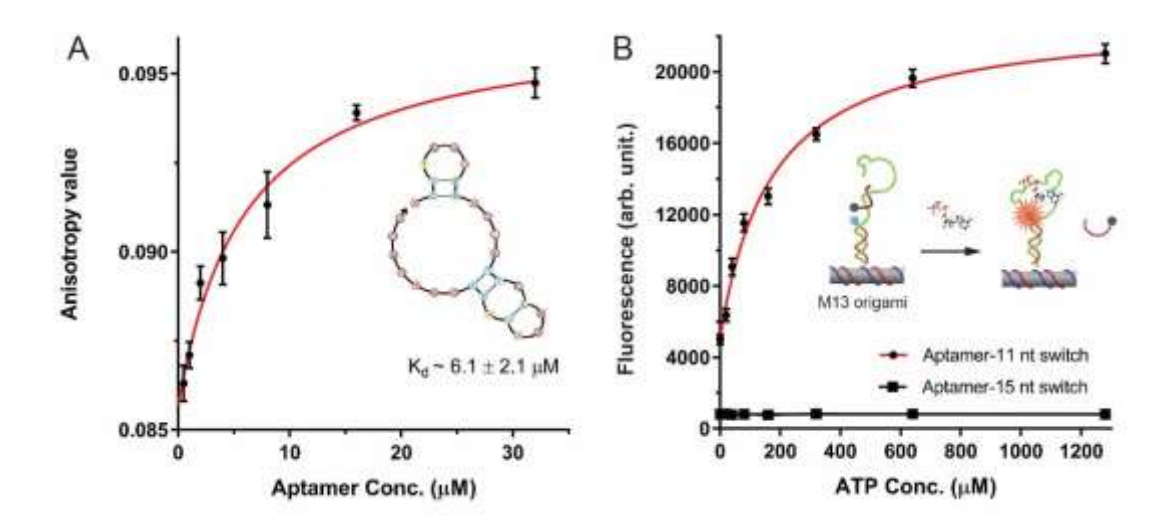


Figure 2. Evaluation of aptamer binding to ATP. (A) Fluorescence anisotropy measurement of an aptamer binding to a Cy3-labelled ATP with a $K_d \sim 6.1 \, \mu M$. (B) Titration of ATP concentrations to disrupt an aptamer-complement duplex on DNA origami surface. Fluorescence increase is observed due to the release of BHQ-labelled complement strand by adding adenosine to disrupt ACDs. As ACD length is increased from 11-nt to 15-nt, apparent Kd values are also increased significantly, and 15-nt ACD is even unable to bind with adenosine. Conditions: 10 nM aptamer in 1×TBS, 2 mM Mg²⁺ buffer. Error bars: the range of data for three replicates.

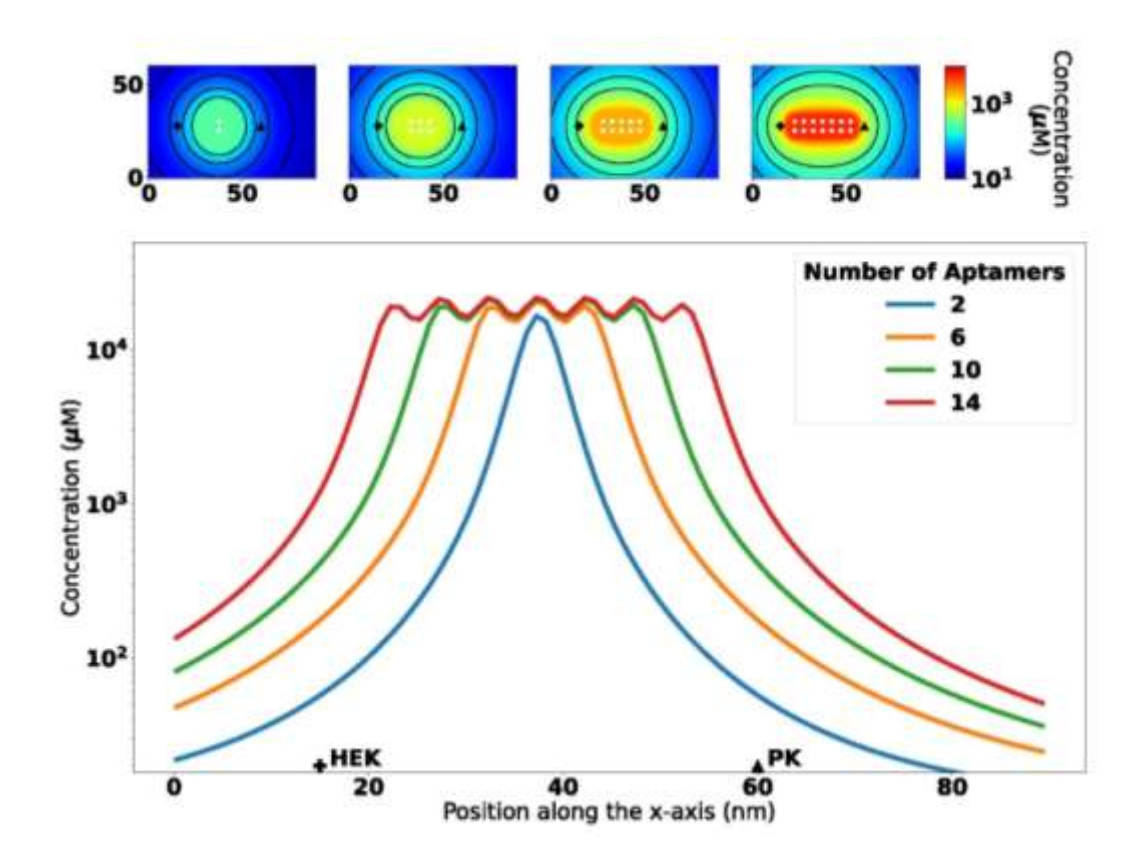


Figure 3. Equilibrium Simulation of ATP enrichment by aptamers on DNA nanostructures.

The concentration gradient as estimated by the equations described in the method with assuming $K_d=10\mu M$, $C_{bulk}=10\mu M$ and a minimal distance of 5 nm. These idealized concentrations are likely to be over-estimated especially very close to aptamers.

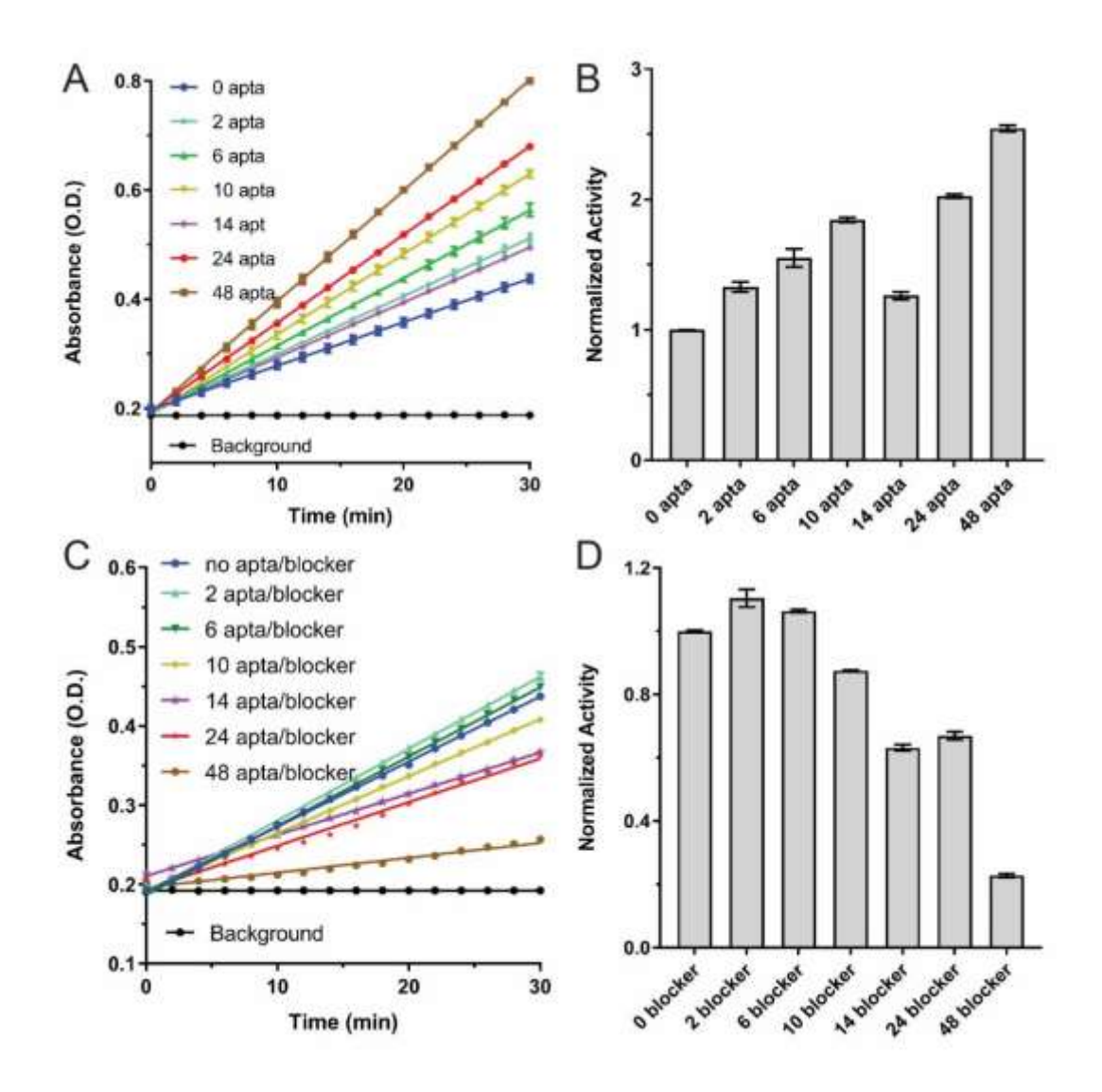


Figure 4. Evaluation of activities for enzyme-assembled DNA structures with modifications of aptamers. (A) Raw activities of enzyme-assembled structures with the modification of aptamers (apta) from 0 to 48, and (B) normalized activities for these structures. (C) Raw activities of enzyme-assembled structures with the modification of aptamer/blocker complexes from 0 to 48, and (D) normalized activities for these structures. Aptamer/blocker complex is the 15-nt aptamer-complement duplex that cannot bind to a ATP. Conditions: 2.5 nM enzyme-DNA nanostructure was assayed with 500 μM mixture of glucose, PEP, NAD⁺, 10 nM G6PDH and 100 μM ADP in 1×TBS, 4 mM Mg²⁺ buffer. Error bars: the range of data for three replicates.

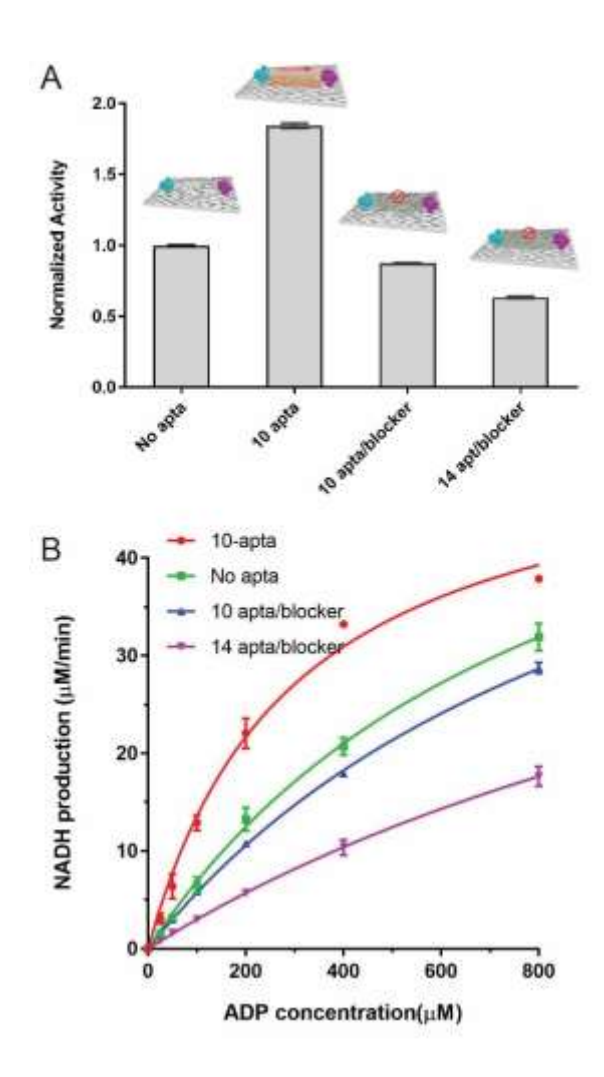


Figure 5. Evaluation of Michaelis constants for assembled enzyme complexes with aptamer modifications. (A) Normalized activities for assembled enzyme complexes with modifications of no aptamer, 10 aptamers, 10 aptamer/blocker duplexes and 14 aptamer/blocker duplexes. (B) Titration of ADP concentrations for producing NADH by assembled PK-HEK complexes with modifications of no aptamer, 10 aptamers, 10 aptamer/blocker duplexes and 14 aptamer/blocker duplexes. Conditions: 2.5 nM enzyme-DNA nanostructure was assayed with 500 μM mixture of glucose, PEP, NAD⁺ and 10 nM G6PDH in pH 7.5, 1×TBS, 4 mM Mg²⁺ buffer. ADP was varied from 0, 12.5, 25, 50, 100, 200, 400 to 800 μM. Error bars: the range of data for three replicates.

Table 1. Fitting of V_{max} , apparent K_M ($K_{M, app}$) and enrichment factor (α) for assembled enzyme structures with different modifications of aptamers and blockers.

	10-apta	No apta	10-apta/blocker	14-apta/blocker
$V_{max}(\mu M/min)$	53.8 ± 2.9	66.2 ± 5.9	66.6 ± 2.3	58.0 ± 9.9
$K_{M, app} (\mu M)$	296 ± 37	860 ± 126	1060 ± 56	1831 ± 418
α	$\sim \! 2.90 \pm 0.32$	1	$\sim 0.81 \pm 0.07$	$\sim 0.47 \pm 0.02$

ASSOCIATED CONTENT

Supporting Information.

Computation model details; DNA origami design (Figure S1); aptamer structures (Figure S2);

titration of Mg²⁺ for enzyme cascade activities (Figure S3): Enzyme co-assembly analysis (Figure

S4, standard curve (Figure S5), titration of enzyme activities (Figure S6-7), thermal annealing

program for preparing DNA nanostructures (Table S1-3), DNA sequences (Table S4-7), (PDF).

AUTHOR INFORMATION

Corresponding Authors

*E-mail: Jinglin Fu, jf604@camden.rutgers.edu

Author Contributions

The manuscript was written through contributions of all authors. All authors have given approval

to the final version of the manuscript.

Notes

The authors declare no competing financial interest.

ACKNOWLEDGMENT

This work was supported by a PECASE award to J.F. (W911NF1910240) and a DoD DURIP

(W911NF2010107). J.F. is also supported by the Rutgers TechAdvance award, NJ-ACTS-Pilot

Program and NSF PFI award (2141141). The authors appreciate the Equipment Leasing Funds

from the State of New Jersey. Authors are also grateful to the inspired discussion with Prof

Henry Hess.

19

REFERENCES

- (1) Fu, J.; Wang, Z.; Liang, X. H.; Oh, S. W.; St Iago-McRae, E.; Zhang, T. DNA-Scaffolded Proximity Assembly and Confinement of Multienzyme Reactions. *Top Curr Chem (Cham)* **2020**, 378, 38.
- (2) Noori, R.; Perwez, M.; Sardar, M. Cross-linked Enzyme Aggregates: Current Developments and Applications. In Husain, Q., Ullah, M. (Eds.) *Biocatalysis: Enzymatic Basics and Applications* **2019**; 83-11, Springer, Cham.
- (3) Xiong, Y.; Tsitkov, S.; Hess, H.; Gang, O.; Zhang, Y. Microscale Colocalization of Cascade Enzymes Yields Activity Enhancement. *ACS Nano* **2022**, *16*, 10383-10391.
- (4) Dueber, J. E.; Wu, G. C.; Malmirchegini, G. R.; Moon, T. S.; Petzold, C. J.; Ullal, A. V.; Prather, K. L. J.; Keasling, J. D. Synthetic protein scaffolds provide modular control over metabolic flux. *Nat. Nanotechnol.* **2009**, *27*, 753-759.
- (5) Singleton, C.; Howard, T. P.; Smirnoff, N. Synthetic metabolons for metabolic engineering. *J Exp Bot* **2014**, *65*, 1947-1954.
- (6) Vriezema, Dennis M.; Garcia, Paula M. L.; Sancho Oltra, N.; Hatzakis, Nikos S.; Kuiper, Suzanne M.; Nolte, Roeland J. M.; Rowan, Alan E.; van Hest, Jan C. M. Positional Assembly of Enzymes in Polymersome Nanoreactors for Cascade Reactions. *Angew. Chem. Int. Ed.* **2007**, *46*, 7378-7382.
- (7) van Dongen, S. F. M.; Nallani, M.; Cornelissen, J. J. L. M.; Nolte, R. J. M.; van Hest, J. C. M. A Three-Enzyme Cascade Reaction through Positional Assembly of Enzymes in a Polymersome Nanoreactor. *Eur. J. Chem.* **2009**, *15*, 1107-1114.
- (8) Kim, K. T.; Meeuwissen, S. A.; Nolte, R. J. M.; van Hest, J. C. M. Smart nanocontainers and nanoreactors. *Nanoscale* **2010**, *2*, 844-858.
- (9) Fiedler, J. D.; Brown, S. D.; Lau, J. L.; Finn, M. G. RNA-Directed Packaging of Enzymes within Virus-like Particles. *Angew. Chem. Int. Ed.* **2010**, *49*, 9648-9651.
- (10) Comellas-Aragones, M.; Engelkamp, H.; Claessen, V. I.; Sommerdijk, N. A. J. M.; Rowan, A. E.; Christianen, P. C. M.; Maan, J. C.; Verduin, B. J. M.; Cornelissen, J. J. L. M.; Nolte, R. J. M. A virus-based single-enzyme nanoreactor. *Nat. Nanotechnol.* **2007**, *2*, 635-639.
- (11) Seeman, N. C. DNA Nanotechnology at 40. Nano Letters **2020**, 20, 1477-1478.
- (12) Madsen, M.; Gothelf, K. V. Chemistries for DNA Nanotechnology. *Chem. Rev.* **2019**, *119*, 6384-6458.
- (13) Jones, M. R.; Seeman, N. C.; Mirkin, C. A. Programmable materials and the nature of the DNA bond. *Science* **2015**, *347*, 1260901.
- (14) Fu, T. J.; Seeman, N. C. DNA double-crossover molecules. *Biochemistry* **1993**, *32*, 3211-3220.
- (15) Rothemund, P. W. K. Folding DNA to create nanoscale shapes and patterns. *Nature* **2006**, 440, 297-302.
- (16) Ke, Y.; Ong, L. L.; Shih, W. M.; Yin, P. Three-Dimensional Structures Self-Assembled from DNA Bricks. *Science* **2012**, *338*, 1177-1183.
- (17) Tian, T.; Li, Y.; Lin, Y. Prospects and challenges of dynamic DNA nanostructures in biomedical applications. *Bone Res* **2022**, *10*, 40.
- (18) DeLuca, M.; Shi, Z.; Castro, C. E.; Arya, G. Dynamic DNA nanotechnology: toward functional nanoscale devices. *Nanoscale Horiz* **2020**, *5*, 182-201.
- (19) Han, D.; Qi, X.; Myhrvold, C.; Wang, B.; Dai, M.; Jiang, S.; Bates, M.; Liu, Y.; An, B.; Zhang, F.; Yan, H.; Yin, P. Single-stranded DNA and RNA origami. *Science* **2017**, *358*, eaao2648.

- (20) Fu, J.; Oh, S. W.; Monckton, K.; Arbuckle-Keil, G.; Ke, Y.; Zhang, T. Biomimetic Compartments Scaffolded by Nucleic Acid Nanostructures. *Small* **2019**, *15*, 1900256.
- (21) Fu, J.; Liu, M.; Liu, Y.; Yan, H. Spatially-Interactive Biomolecular Networks Organized by Nucleic Acid Nanostructures. *Acc. Chem. Res.* **2012**, *45*, 1215-1226.
- (22) Wilner, O. I.; Weizmann, Y.; Gill, R.; Lioubashevski, O.; Freeman, R.; Willner, I. Enzyme cascades activated on topologically programmed DNA scaffolds. *Nat. Nanotechnol.* **2009**, *4*, 249-254.
- (23) Fu, J.; Liu, M.; Liu, Y.; Woodbury, N. W.; Yan, H. Interenzyme Substrate Diffusion for an Enzyme Cascade Organized on Spatially Addressable DNA Nanostructures. *J. Am. Chem. Soc.* **2012**, *134*, 5516-5519.
- (24) Fu, Y.; Zeng, D.; Chao, J.; Jin, Y.; Zhang, Z.; Liu, H.; Li, D.; Ma, H.; Huang, Q.; Gothelf, K. V.; Fan, C. Single-Step Rapid Assembly of DNA Origami Nanostructures for Addressable Nanoscale Bioreactors. *J. Am. Chem. Soc.* **2013**, *135*, 696-702.
- (25) Fu, J.; Yang, Y. R.; Johnson-Buck, A.; Liu, M.; Liu, Y.; Walter, N. G.; Woodbury, N. W.; Yan, H. Multi-enzyme complexes on DNA scaffolds capable of substrate channelling with an artificial swinging arm. *Nat. Nanotechnol.* **2014**, *9*, 531-536.
- (26) Ke, G.; Liu, M.; Jiang, S.; Qi, X.; Yang, Y. R.; Wootten, S.; Zhang, F.; Zhu, Z.; Liu, Y.; Yang, C. J.; Yan, H. Directional Regulation of Enzyme Pathways through the Control of Substrate Channeling on a DNA Origami Scaffold. *Angew. Chem. Int. Ed.* **2016**, *55*, 7483-7486.
- (27) Yang, Y. R.; Fu, J.; Wootten, S.; Qi, X.; Liu, M.; Yan, H.; Liu, Y. 2D Enzyme Cascade Network with Efficient Substrate Channeling by Swinging Arms. *ChemBioChem* **2018**, *19*, 212-216.
- (28) Sprengel, A.; Lill, P.; Stegemann, P.; Bravo-Rodriguez, K.; Schöneweiß, E.-C.; Merdanovic, M.; Gudnason, D.; Aznauryan, M.; Gamrad, L.; Barcikowski, S.; Sanchez-Garcia, E.; Birkedal, V.; Gatsogiannis, C.; Ehrmann, M.; Saccà, B. Tailored protein encapsulation into a DNA host using geometrically organized supramolecular interactions. *Nat. Commun.* **2017**, *8*, 14472.
- (29) Grossi, G.; Dalgaard Ebbesen Jepsen, M.; Kjems, J.; Andersen, E. S. Control of enzyme reactions by a reconfigurable DNA nanovault. *Nat. Commun.* **2017**, *8*, 992.
- (30) Zhao, Z.; Fu, J.; Dhakal, S.; Johnson-Buck, A.; Liu, M.; Zhang, T.; Woodbury, N. W.; Liu, Y.; Walter, N. G.; Yan, H. Nanocaged enzymes with enhanced catalytic activity and increased stability against protease digestion. *Nat. Commun.* **2016**, *7*, 10619.
- (31) Zhang, Y.; Hess, H. Toward Rational Design of High-efficiency Enzyme Cascades. *ACS Catal.* **2017**, *7*, 6018-6027.
- (32) Lin, J.-L.; Wheeldon, I. Kinetic Enhancements in DNA–Enzyme Nanostructures Mimic the Sabatier Principle. *ACS Catal.* **2013**, *3*, 560-564.
- (33) Lin, J.-L.; Palomec, L.; Wheeldon, I. Design and Analysis of Enhanced Catalysis in Scaffolded Multienzyme Cascade Reactions. *ACS Catal.* **2014**, *4*, 505-511.
- (34) Gao, Y.; Roberts, C. C.; Zhu, J.; Lin, J.-L.; Chang, C.-e. A.; Wheeldon, I. Tuning Enzyme Kinetics through Designed Intermolecular Interactions Far from the Active Site. *ACS Catal.* **2015**, *5*, 2149-2153.
- (35) Gao, Y.; Roberts, C. C.; Toop, A.; Chang, C.-e. A.; Wheeldon, I. Mechanisms of Enhanced Catalysis in Enzyme–DNA Nanostructures Revealed through Molecular Simulations and Experimental Analysis. *ChemBioChem* **2016**, *17*, 1430-1436.

- (36) Golub, E.; Albada, H. B.; Liao, W.-C.; Biniuri, Y.; Willner, I. Nucleoapzymes: Hemin/G-Quadruplex DNAzyme–Aptamer Binding Site Conjugates with Superior Enzyme-like Catalytic Functions. *J. Am. Chem. Soc.* **2016**, *138*, 164-172.
- (37) Hu, Y.; Wang, F.; Lu, C.-H.; Girsh, J.; Golub, E.; Willner, I. Switchable Enzyme/DNAzyme Cascades by the Reconfiguration of DNA Nanostructures. *Eur. J. Chem.* **2014**, *20*, 16203-16209.
- (38) Saghatelian, A.; Guckian, K. M.; Thayer, D. A.; Ghadiri, M. R. DNA Detection and Signal Amplification via an Engineered Allosteric Enzyme. *J. Am. Chem. Soc.* **2003**, *125*, 344-345.
- (39) Mukherjee, P.; Leman, L. J.; Griffin, J. H.; Ghadiri, M. R. Design of a DNA-Programmed Plasminogen Activator. *J. Am. Chem. Soc.* **2018**, *140*, 15516-15524.
- (40) Janssen, B. M. G.; Engelen, W.; Merkx, M. DNA-Directed Control of Enzyme–Inhibitor Complex Formation: A Modular Approach to Reversibly Switch Enzyme Activity. *ACS Synth. Biol.* **2015**, *4*, 547-553.
- (41) Oh, S. W.; Pereira, A.; Zhang, T.; Li, T.; Lane, A.; Fu, J. DNA-Mediated Proximity-Based Assembly Circuit for Actuation of Biochemical Reactions. *Angew. Chem. Int. Ed.* **2018**, *57*, 13086-13090.
- (42) Liu, M.; Fu, J.; Hejesen, C.; Yang, Y.; Woodbury, N. W.; Gothelf, K.; Liu, Y.; Yan, H. A DNA tweezer-actuated enzyme nanoreactor. *Nat. Commun.* **2013**, *4*, 2127.
- (43) Collins, J.; Zhang, T.; Oh, S. W.; Maloney, R.; Fu, J. DNA-crowded enzyme complexes with enhanced activities and stabilities. *ChemComm* **2017**, *53*, 13059-13062.
- (44) Fu, J.; Yang, Y. R.; Dhakal, S.; Zhao, Z.; Liu, M.; Zhang, T.; Walter, N. G.; Yan, H. Assembly of multienzyme complexes on DNA nanostructures. *Nat. Protocols* **2016**, *11*, 2243-2273.
- (45) Larsen, T. M.; Benning, M. M.; Rayment, I.; Reed, G. H. Structure of the Bis(Mg²⁺)–ATP–Oxalate Complex of the Rabbit Muscle Pyruvate Kinase at 2.1 Å Resolution: ATP Binding over a Barrel. *Biochemistry* **1998**, *37*, 6247-6255.
- (46) Diderich, J. A.; Raamsdonk, L. M.; Kruckeberg, A. L.; Berden, J. A.; Van Dam, K. Physiological Properties of Saccharomyces cerevisiae from Which Hexokinase II Has Been Deleted. *Appl. Environ. Microbiol.* **2001**, *67*, 1587-1593.
- (47) Xia, T.; Yuan, J.; Fang, X. Conformational Dynamics of an ATP-Binding DNA Aptamer: A Single-Molecule Study. *J. Phys. Chem. B* **2013**, *117*, 14994-15003.
- (48) Huizenga, D. E.; Szostak, J. W. A DNA Aptamer That Binds Adenosine and ATP. *Biochemistry* **1995**, *34*, 656-665.

Table of Contents Graphic

